Biomaterials 31 (2010) 8371–8381

Contents lists available at ScienceDirect

Biomaterials

journal homepage: www.elsevier.com/locate/biomaterials

# Chitosan-based responsive hybrid nanogels for integration of optical pH-sensing, tumor cell imaging and controlled drug delivery

Weitai Wu [a], Jing Shen [a], Probal Banerjee [a,b], Shuiqin Zhou [a,*]

[a] Department of Chemistry, College of Staten Island, and The Graduate Center, The City University of New York, Staten Island, NY 10314, USA
[b] CSI/IBR Center for Developmental Neuroscience, College of Staten Island, and The Graduate Center, The City University of New York, Staten Island, NY 10314, USA

ARTICLE INFO

*Article history:*
Received 26 April 2010
Accepted 15 July 2010
Available online 10 August 2010

*Keywords:*
Chitosan
Hydrogel
Quantum dots
Biosensor
Tumor cell imaging
Drug delivery

ABSTRACT

We report a new class of chitosan-based hybrid nanogels by in-situ immobilization of CdSe quantum dots (QDs) in the chitosan–poly(methacrylic acid) (chitosan–PMAA) networks. The covalently crosslinked hybrid nanogels with chitosan chains semi-interpenetrating in the crosslinked PMAA networks exhibit excellent colloidal and structural stability as well as reversible physical property change in response to a pH variation cross the physiological condition. In contrast, the hybrid nanogels formed by non-covalent physical association exhibit a significant change in the structure and composition upon exposure to physiological pH. This distinction in the structural stability of hybrid nanogels produces very different outcomes for their biomedical applications. The covalently crosslinked hybrid nanogels are low-cytotoxic and could illuminate the B16F10 cells, sense the environmental pH change, and regulate the release of anticancer drug in the typical abnormal pH range of 5–7.4 found in pathological zone, thus successfully combine multiple functionality into a single nano-object. However, the physically associated hybrid nanogels exhibit a non-reversible pH-sensitive PL property and a significant cytotoxicity after 24 h treatment. It is critical to construct a highly stable biopolymer-QD hybrid nanogel, via a rational design for safe bionanomaterials, to simultaneously combine the biosensing, bioimaging, and effective therapy functions.



## 1. Introduction

The application of nanotechnology to biological science is widely expected to change the landscape of pharmaceutical and biotechnology industries for the foreseeable future. After significant advances in the fabrication of a wide variety of functional nanomaterials, it has seen increasing interest in the incorporation of multiple functionalities into a single nano-object [1–13]. Quantum dots (QDs) have been intensively explored for bioimaging and labeling probes due to their unique optical properties, including wideband excitation, narrow emission, phenomenal photostability, high quantum yield, and potential for simultaneous multicolor imaging [1–8]. To combine the imaging ability with the therapy function, much work has focused on the surface conjugation of QDs with biocompatible ligands, such as peptides, antibodies, and biopolymers [9–13]. However, the monolayer capped QDs usually have low drug loading capacity and are lack of sensitivity to control the drug release in response to local environmental change. On the other hand, stimuli-responsive microgels/nanogels offer unique advantages as drug delivery carriers, including a tunable size from submicrons to tens of nanometers, large surface area for bioconjugation, porous structure for storage of therapeutics, and controllable drug release at specific chemical and biological environment [14–17]. A single nano-object with the immobilization of QDs in the interior of responsive nanogels is undoubtedly of special interest to integrate the optical sensing [18–22], imaging diagnostics [1,3], and controlled drug release [15] because of their unique stimuli-responsive volume phase transition, visible luminescence, and porosity.

Natural biopolymers have been widely used to prepare responsive hydrogels for biomedical application due to their biocompatibility, low toxicity, and a high content of functional groups [23–28]. Although significant benefits have been achieved on the relative areas, to the best of our knowledge, few studies refer to the natural biopolymer-based bionanomaterials for simultaneous sensing, imaging diagnosis and therapy. We recently presented a multifunctional system on the basis of immobilization of QDs into the hydroxypropylcellulose–poly(acrylic acid) (HPC–PAA) semi-interpenetrating (semi-IPN) nanogel for simultaneous optical pH-sensing, tumor cell imaging, and pH-regulated delivery of

* Corresponding author. Tel.: +1 718 982 3897; fax: +1 718 982 3910.
*E-mail address:* shuiqin.zhou@csi.cuny.edu (S. Zhou).

0142-9612/$ – see front matter © 2010 Elsevier Ltd. All rights reserved.
doi:10.1016/j.biomaterials.2010.07.061

anticancer drug [29]. Despite of the exciting conception, several key issues remain unaddressed in this system. First, the pH-responsive optical tracing and drug release only demonstrate high sensitivity in the pH range from 4 to 6, while many pathological processes in various tissues and organs are accompanied with local pH decrease by 1–2.5 pH units (acidosis) and/or temperature increase by 1–5 °C [30–32]. Second, the HPC–PAA–QD hybrid nanogel system is not suitable for long circulation at pH < 5.5 and $T > 37$ °C, because the HPC–PAA semi-IPN networks would adopt a compact structure with high hydrophobicity under these conditions, thus cause a potential aggregation. Third, it is necessary to examine whether the synthetic strategy of in-situ immobilization of QDs into responsive polysaccharide-based nanogels is generally applicable to other type of polysaccharide-based nanogels. At last, the stability of the morphology and composition of the polysaccharide-QD hybrid nanogels under physiological important pH range should be another critical factor for the designed multiple functionality, thus, need be investigated to implement a rational approach for the safe design of bionanomaterials.

Here, we develop a class of chitosan-based hybrid nanogels ($R_h$ < 100 nm) with CdSe QDs (3.2–3.8 nm) in-situ immobilized in the chitosan–poly(methacrylic acid) (chitosan–PMAA) semi-IPN networks, which should display the properties and functions from each building blocks, as schematically depicted in Fig. 1. Chitosan is distinct from other commonly available polysaccharides due to its glucosamine groups, cationicity, and capacity to form polyelectrolyte complexes, making it a very versatile material with extensive application in the biomedical and biotechnological fields [26,27]. Some studies have revealed that chitosan might function as an immune adjuvant, demonstrating that chitosan of a high degree of deacetylation is a promising and safe platform for parenteral drug delivery [33–35]. In addition, the rich –OH groups of chitosan chains should be able to sequester $Cd^{2+}$ ions into the gel network and stabilize the in-situ formed CdSe QDs embedded in the gel network. In order to fabricate chitosan–PMAA–CdSe hybrid nanogels, we prepared chitosan–PMAA semi-IPN nanogels with two strategies. One is totally through the non-covalent physical chitosan–PMAA chain associations, such as secondary forces (ionic, hydrogen or hydrophobic bonding) and physical entanglements. Another is through the covalent crosslinkage of PMAA with chitosan semi-interpenetrated in the PMAA networks. Both chitosan ($pK_a$ ~ 6.5) and PMAA chains ($pK_a$ ~ 5.5) are pH-sensitive. While the CdSe QDs are designed as an optical identification code for biosensing and cellular imaging, the reversible pH-induced volume phase transitions of the chitosan–PMAA nanogels will modify the physicochemical environment of the embedded QDs for converting chemical/biochemical signals to optical signals and regulate the release of anticancer drug temozolomide (TMZ) trapped in the gels in the typical abnormal pH range of 5–7.4 found in microenvironments of extracellular tissues of tumors [29–32]. The structural and composition stability of the hybrid nanogels synthesized from covalent crosslinking method and physical association method at various environmental pH was investigated and compared, which were further correlated to the pH-regulated physical properties, toxicity, and functionalities of these hybrid nanogels. The rationally designed biopolymer-based hybrid nanogels that can integrate the pH-sensing, cancer cellular imaging, and intelligently dosing the pathological zone under the local environmental stimuli hold a great promise for simultaneous diagnosis, therapy, and monitoring on the response to drug treatments.

## 2. Materials and methods

### 2.1. Materials

Chitosan ($M_r$ ~ 150, 000) was purchased from Fluka, and other chemicals were purchased from Aldrich. Chitosan was purified by dissolving in a 1 wt% acetic acid solution, filtration, re-precipitation in 1.0 M NaOH solution, and then washed and dried in a vacuum at room temperature. The purified chitosan has a deacetylation degree of about 90.2% as determined by titration. MAA was purified by distillation under reduced pressure to remove inhibitors. Selenium (Se), sodium sulfite ($Na_2SO_3$), cadmium chloride hydrate ($CdCl_2 \cdot xH_2O$), NaOH, 0.1 N HCl standard solution, *N*,*N*′-methylenebisacrylamide (MBAAm), ammonium persulfate (APS), and TMZ were used as received without further purification. The water used in all experiments was of Millipore Milli-Q grade.

### 2.2. Synthesis of chitosan–PMAA–CdSe hybrid nanogels

#### 2.2.1. Synthesis of chitosan–PMAA nanogels

To synthesize chitosan–PMAA nanogels, purified chitosan was solubilized into 100 mL MAA solution at a given MAA/aminoglucoside molar ratio (Table 1) under magnetic stirring for 12 h in a 250 mL three-neck round-bottom flask equipped with a $N_2$ gas inlet and a condenser. The crosslinker MBAAm was then added. The mixture was slowly heated to 60 °C under a $N_2$ purge. After 30 min, 1 mL of 0.122 M APS was added to initiate the polymerization. The reaction was allowed to proceed for 1 h. The resultant nanogel was filtered through a Millipore Millex-HV filter with a pore size of 1.0 μm to remove any possible aggregation, and then purified by 3 days of dialysis (Spectra/Por® molecularporous membrane tubing, cutoff 12000–14000, the same below) against very frequently changed dilute HCl solution of pH ~ 4.8 ± 0.2 at room temperature.

#### 2.2.2. In-situ synthesis of CdSe QDs in chitosan–PMAA nanogels

After adjusting the pH to 4.6–5.0, 100 mL chitosan–PMAA nanogel dispersions were stirred in a 250 mL glass vial for 30 min. A solution of $CdCl_2 \cdot xH_2O$ (3.5 wt%, 5 mL) was added dropwisely to the vial. The mixture was stirred at room temperature for 1 day. After that, excess $Cd^{2+}$ was removed by centrifugation, decantation, and dialysis against very frequently changed water for 2 days. In the whole process, the solution was kept in acidic condition of pH ~ 4.6–5.0. The nanogels loaded with $Cd^{2+}$ ions were poured into a 250 mL round-bottom flask equipped with a stirrer, a $N_2$ gas inlet, and a condenser. After 30 min $N_2$ purge, 6.5 mL fresh $Na_2SeSO_3$ solution (0.335 M) [29] was dropwisely added. The temperature was rapidly raised to 100 °C, and the mixture gradually turned to brilliant yellow, orange and finally red color [36–38]. The mixture was further stirred for 30 min until the color was stable. The resulted nanogels incorporated with CdSe QDs were cooled down under $N_2$ atmosphere, and then purified by centrifugation, decantation, and dialysis against

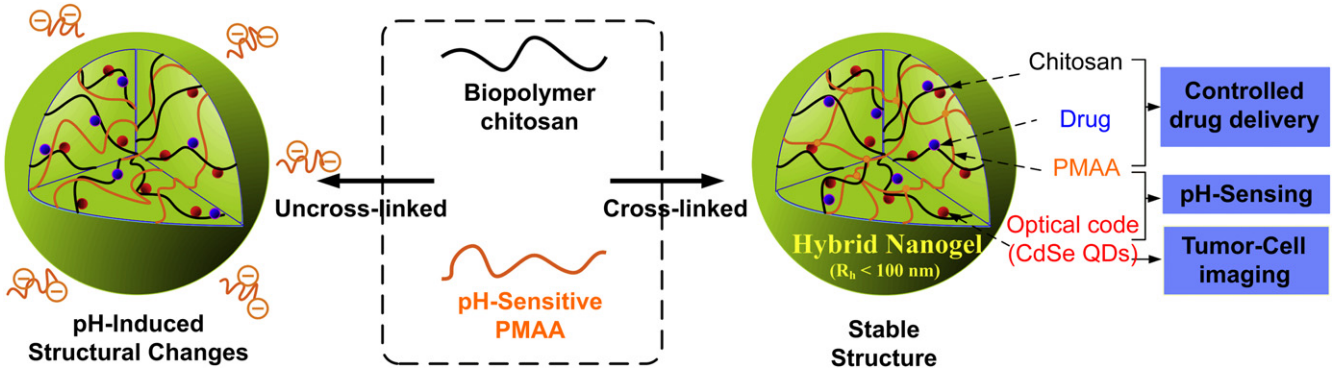


**Fig. 1.** Schematic representation of the concept for designing multifunctional chitosan–PMAA–CdSe hybrid nanogel and its potential extending applications in biomedical field.

**Table 1**
Dependence of particle size on feeding ratios of chitosan/MAA/MBAAm.

| Chitosan/MAA /MBAAm[a] (wt/wt/wt) | Diameter[b] (nm) | Polydispersity | Zeta potential[b] (mV) |
|---|---|---|---|
| 100:210:15 | 174.5 | 0.109 | −23.1 ± 2.4 |
| 100:105:15 | 119.8 | 0.098 | −9.6 ± 2.0 |
| 100:79:15 | 104.2 | 0.084 | −3.3 ± 1.8 |
| 100:53:15 | 74.7 | 0.055 | −1.9 ± 0.6 |
| 100:53:0 | 84.6 | 0.127 | −1.2 ± 0.8 |

[a] The concentration of chitosan was fixed at $1.03 \times 10^{-3}$ g/mL.
[b] Measured in an acidic medium (pH ~ 5.0) at 22.1 °C.

very frequently changed water (pH ~ 4.6–5.0) at room temperature for 3 days. The samples were stored at 3 °C for further studies.

### 2.3. Stability studies of hybrid nanogels

To study the stability of the hybrid nanogels during their storage under constant conditions (3 °C and pH ~ 4.8 ± 0.2), the distribution of hydrodynamic radius (*R*h) was measured at defined time periods. To study the effect of pH change on the stability of hybrid nanogels, 5 mL hybrid nanogels purified at pH ~ 4.8 ± 0.2 in a dialysis bag were exposed to 50 mL phosphate buffer solution (PBS) of pH 7.38 at 37 °C. The dispersion inside the dialysis bag was sampled at defined time periods and analyzed by FTIR spectrometry, transmission electron microscopy (TEM), and light scattering to monitor their composition, morphology, and size change.

### 2.4. Incorporation of the hybrid nanogels into mouse melanoma B16F10 cells

Round glass coverslips were placed in each well of a 24-well plate and treated with 0.1% poly-L-lysine in 100 mM PBS for 40 min. Following the treatment, the solution was aspirated and the wells were washed with PBS three times. Next, B16F10 cells ($2 \times 10^4$ cell/well) were seeded on the glass coverslips at 80% confluence in Dulbecco's modified Eagle's medium (DMEM) containing 10% fatal bovine serum (FBS) and 1% penicillin–streptomycin. On the next day, each sample was diluted to three concentrations in serum-free DMEM in the following manner: (i) 50 μL of sample (0.75 μg) with 450 μL serum-free DMEM; (ii) 100 μL of sample (1.5 μg) with 400 μL serum-free DMEM; (iii) 200 μL sample (3 μg) with 300 μL serum-free DMEM. Additionally, 500 μL of serum-free medium was added to a control well. Each of the diluted samples in 500 μL medium was added to a marked well. 500 μL of serum-free medium was added to the control well. After incubated at 37 °C for 2 h, the medium was aspirated and fresh serum-free DMEM was added to each well. Finally, the coverslips with cells were removed from the wells and mounted onto slides with mounting fluid.

### 2.5. Drug loading and in vitro release

TMZ was loaded into the hybrid nanogels by using complexation method. 5 mL hybrid nanogel dispersion with pH adjusted to 4.3 was stirred in an ice water bath for 30 min. 500 μL of TMZ solution (1 mg/mL, pH = 3.0) was then added dropwisely to the vial. After stirring overnight, the suspension was centrifuged for 20 min at 10000 rpm and room temperature. To remove free TMZ, the precipitate was redispersed in 5 mL HCl solution of pH = 4.3, and further purified by centrifugation and washing several times. All the upper clear solutions were collected, and the concentration of free TMZ was determined by UV–vis spectrometry at 328 nm. The amount of loaded TMZ in the hybrid nanogels was calculated from the decrease in TMZ concentration. The loading content is expressed as the mass of loaded drug per unit weight of dried hybrid nanogels.

The *in vitro* release behavior was evaluated by the dialysis method. 5 mL of purified TMZ-loaded hybrid nanogel dispersion (pH = 2.0) was placed inside a dialysis bag, which was immersed in 50 mL 0.005 M buffer solutions of different pH values of 7.38, 6.67, 6.15, and 5.03, respectively. The released TMZ outside of the dialysis bag was sampled at defined time period and assayed by UV–vis absorption at both 328 nm (TMZ) and 266 nm (degradation product), based on the linear calibration curve with $R^2 > 0.99$ under the same condition. Cumulative release is expressed as the total percentage of drug released through the dialysis membrane over time.

### 2.6. In vitro cytotoxicity

B16F10 cells (2000 cell/well) were cultured in DMEM containing 10% FBS and 1% penicillin–streptomycin in two 96-well plates, and exposed to free TMZ, drug-free chitosan–PMAA–CdSe hybrid nanogels, and TMZ-loaded chitosan–PMAA–CdSe hybrid nanogels. To cover the high concentrations, the nanogels were concentrated and adjusted to an appropriate concentration in DMEM right before feeding into the well. One plate was incubated at 37 °C for 2 h and another plate was incubated for 24 h. The medium was then aspirated, and these wells were washed using fresh serum-free DMEM. After that, 25 μL of 3-(4,5-dimethyl-2-thiazolyl)-2,5-diphenyltetrazolium bromide (MTT) solution (5 mg/mL in PBS) were added to the wells. After incubation for 2 h, the solution was aspirated. 100 μL of dimethyl sulfoxide was then added to each well and the plate was sealed and incubated for 30 min at 37 °C with gentle mixing. Three portions of the solution obtained from each well were transferred to three respective wells of a 96-well plate. Cell viability was measured using a microplate reader at 570 nm. Positive controls contained no TMZ or nanogels, and negative controls contained MTT.

### 2.7. Characterization

The FTIR spectra were recorded with a Nicolet Instrument Co. MAGNA-IR 750 Fourier transform infrared spectrometer. The UV–vis absorption spectra were obtained on a Thermo Electron Co. Helios β UV–vis Spectrometer. The photoluminescence (PL) spectra were obtained on a JOBIN YVON Co. FluoroMax®-3 Spectrofluorometer equipped with a R928P photomultiplier tube and confirmed on a VARIAN CARY Eclipse Spectrofluorometer equipped with R928 photomultiplier tubes and self-optimized light filters. The pH values were measured on a METTLER TOLEDO SevenEasy pH meter. The TEM images were taken on a FEI TECNAI transmission electron microscope at an accelerating voltage of 120 kV to examine the morphology of hybrid nanogels. The confocal scanning microscopy (LEICA TCS SP2 AOBS™), with an Argon laser (496 nm) as the light source, was applied to image the cell morphology and distributions of the hybrid nanogels in the cells. A standard laser light scattering spectrometer (BI-200SM) equipped with a BI-9000 AT digital time correlator and a He–Ne laser (35 mW, 633 nm) was used to determine the size and size distributions of hybrid nanogels at a scattering angle of 45° and the molecular weight ($M_w$) of PMAA chains [39]. The zeta potential measurements were carried out on a Zeta-Meter mode and calibrated with standard solutions.

## 3. Results and discussion

### 3.1. Synthesis of chitosan–PMAA–CdSe hybrid nanogels

Our strategy to prepare the multifunctional chitosan–PMAA–CdSe hybrid nanogels involves the first synthesis of stimuli-responsive chitosan–PMAA semi-IPN nanogels, followed by the in-situ synthesis of CdSe QDs inside the nanogels. The chitosan–PMAA semi-IPN nanogels were prepared by the polymerization of MAA monomers in chitosan aqueous solution in the presence and absence of crosslinker MBAAm. Chitosan chain in solution is in cationic polyelectrolyte form, which tends to ease the formation of specific structures via electrostatic interactions with MAA molecules and form interpolymer complexes [40,41]. The polymerization and crosslinking of the MAA monomers that are complexed with chitosan chains can result in narrowly distributed gel particles with a chemically crosslinked PMAA network semi-interpenetrated by chitosan chains. The interplay of other interactions, such as hydrophobic association of methyl groups of PMAA chains, may also contribute towards the stability of the nanogels. The size and zeta potential of the chitosan–PMAA nanogels could be simply controlled by tuning the feeding ratio of MAA/chitosan (Table 1). The mean diameter of chitosan–PMAA nanogels varies from 174.5 to 74.7 nm when the MAA/chitosan ratio changes from 2.10 to 0.53. The chitosan–PMAA nanogel formed totally by physical chain associations shows a broader size distribution compared to the corresponding covalently crosslinked nanogel prepared under the same conditions. The nanogels presented negative surface charge at pH ≈ 5.0. The zeta potential tended to be neutral as the MAA/chitosan ratio decreased. Although PMAA chains show a theta temperature $\Theta$ of 30 °C in aqueous solution of low pH [42], all nanogels were well dispersed in water without precipitation for several months at room temperature due to the dominant hydrophilic nature of chitosan.

On the basis of physiological parameters such as hepatic filtration, tissue extravasation, tissue diffusion, and kidney excretion, it is clear that particle size is a key factor in the biodistribution of long-circulating nanoparticles and achieving therapeutic efficacy [43]. The nanoparticle carriers in the size range of 10–100 nm have actual advantages to improve the blood circulation time and enhance the extravasation rate into permeable tissues such as

tumors [28,43–45]. Herein, three small-sized chitosan–PMAA nanogels with chitosan/MAA/MBAAm = 100: 79: 15, 100:53: 15, and 100: 53: 0, and corresponding hydrodynamic diameter of 104.2, 74.7, and 84.6 nm (Table 1) were selected for further immobilization of CdSe QDs. The resulting hybrid nanogels are coded as CPM1, CPM2, and CPM3, respectively. Both the $-COO^-$ groups of PMAA and the $-NH_2$ and $-OH$ groups of chitosan are able to link metal ions and QDs [14,17–22]. Our motivation is to use the $-OH$ groups of chitosan chains to bind the $Cd^{2+}$ ions into the nanogels and to protect the resultant CdSe QDs from agglomeration or release, but protect the $-NH_2$ and $-COO^-$ groups mainly used for inducing pH-responsive volume phase transition of nanogels. To reach this purpose, the whole uptake process of $Cd^{2+}$ ions into the nanogels was carried out in acidic medium of pH $\sim 4.8 \pm 0.2$, which is below the $pK_a = 5.5$ for PMAA and $pK_a = 6.5$ for chitosan, respectively. With such a specific pH design, the PMAA chains have little ionized $COO^-$ groups ($pH < pK_a$) for uptake of $Cd^{2+}$ ions, while the amino groups of chitosan are mostly protonated ($pH < pK_a$) and positively charged, thus will not bind the $Cd^{2+}$ ions. Therefore, most of $Cd^{2+}$ ions are loaded into the nanogels through the coordination between the $Cd^{2+}$ ions and the $-OH$ groups of chitosan chains. After the uptake of $Cd^{2+}$ ions into the nanogels, the excess $CdCl_2$ in the external solution was removed by centrifugation, decantation, and dialysis against a dilute HCl solution of pH $\sim 4.8 \pm 0.2$. This procedure is designed to make sure that CdSe QDs can only be formed inside the chitosan–PMAA nanogels. The synthetic mechanism of CdSe QDs in aqueous media at low temperatures has been investigated [36]. As expected, the in-situ immobilization of the CdSe QDs into the nanogels almost has no effect on the characteristic absorption peaks of $-COOH$ groups of PMAA (1718 $cm^{-1}$) and amide bands of chitosan (1580–1650 $cm^{-1}$) in FTIR spectra (Fig. 2) due to the successful protection of these functional groups during the loading process of $Cd^{2+}$ ions. In comparison with the chitosan–PMAA template nanogel, the disappeared peak at 1211 $cm^{-1}$ and the emerged new signal at 1145 $cm^{-1}$ for the chitosan–PMAA–CdSe hybrid nanogels can be associated with the binding of CdSe QDs with oxygenic groups of chitosan.

Fig. 3 shows the TEM images of the chitosan–PMAA–CdSe hybrid nanogels in acid medium (pH $\approx$ 5.0). The QDs were randomly distributed throughout the whole volume of all the chitosan–PMAA–CdSe hybrid nanogels. As the size of semiconductor nanocrystals is directly related to the excitonic peak in the UV–vis absorption spectrum, the size of the CdSe QDs can be estimated by empirical mathematical functions reported by Peng's group [46]. Peaks observed around 560–580 nm (Fig. 4) for the three hybrid nanogels are assigned to the 1s–1s electronic transitions, from which the average particle size was determined to be 3.2–3.8 nm. Thus the CdSe particles exhibit extremely strong quantum confinement in all the chitosan–PMAA–CdSe hybrid nanogels. Moreover, no significant change in size was observed after 6 months' storage.

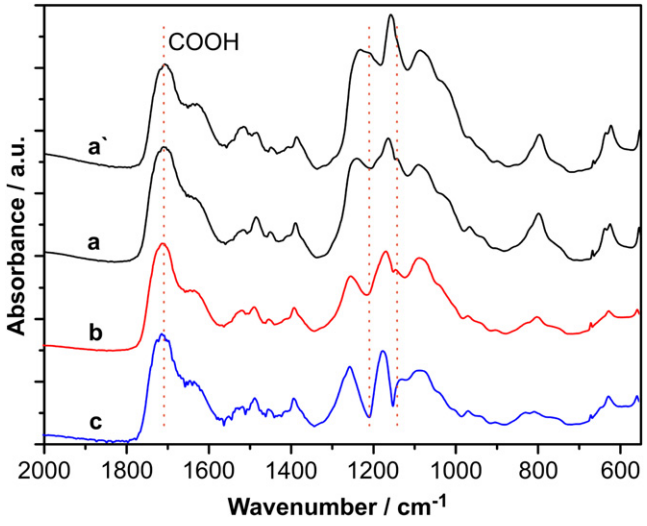


**Fig. 2.** Typical FTIR spectra of chitosan–PMAA–CdSe hybrid nanogels synthesized with chitosan/MAA/MBAAm = 100: 79: 15 (a, CPM1), 100: 53: 15 (b, CPM2), and 100: 53: 0 (c, CPM3), respectively. The FTIR spectrum of the chitosan–PMAA nanogel template corresponding to CPM1 was also shown for comparison (a′).

### 3.2. Volume phase transitions and stability of Chitosan–PMAA–CdSe hybrid nanogels

Fig. 5 shows the pH-induced swelling curves of the chitosan–PMAA–CdSe hybrid nanogels, in terms of the $R_h$ change measured at $T = 22.1$ °C and 37.2 °C, respectively. Although the formation of chitosan–PMAA complex particles has recently attracted intensive interests [40,41], the volume phase behavior of the complexes is rarely studied in detail. As expected, our hybrid nanogels exhibited marked swelling at both high and low pH values, but a minimum size at pH $\sim$ 5.0–5.5. The swelling of the hybrid nanogels containing pH-responsive groups is governed by the internal osmotic pressure due to the mobile counter-ions contained within the particles, which balance the internal electrostatic repulsion. At high pH values (e.g. >8.0), the nanogels remained nearly a maximum swelling degree due to the high degree ionization of $-COO^-$ groups of PMAA chains. With a decrease in pH, the $-COO^-$ groups gradually protonate to $-COOH$, which cannot only enhance the hydrogen bonding interactions between the chitosan and PMAA chains, but also reduce the Coulombic repulsion within the particles, resulting in the gradual decrease in the size of hybrid nanogels. When pH is decreased to the $pK_a$ of chitosan, the $-NH_2$ groups of chitosan will be gradually protonated. Because a much lower pH (<4.8) is needed to make the full protonation of the carboxyl groups [42], PMAA chains are still partially negatively charged at pH $\approx$ 5.0–6.5, which can produce electrostatic attraction with the positively charged $-NH_3^+$ groups of chitosan, thus further reduce the size of nanogels. Because the molar ratio of MAA-to-glucosamine is larger than 2.24 in these hybrid nanogels, an increased acidity is required to protonate the excess $-COO^-$ groups that are not neutralized by $-NH_3^+$ groups until reaching the isoelectric point (pH $\approx$ 5–5.5), at which the largest contraction of the gel network chains occurred. Further decreasing pH to below 5, the overall charges of the hybrid nanogels convert to positive due to the excess $-NH_3^+$ groups. The increased charge density on the gel built up a Donnan potential for the gel to swell steadily in a more acidic medium. The temperature has negligible effect on the pH-induced two-way volume phase transition of the hybrid nanogels. However, the size of the hybrid nanogels measured at 37.2 °C is generally larger than that at 22.1 °C over the whole investigated pH window, which could be attributed to the unique thermo-responsive phase behavior of PMAA in water ($\Theta \approx 30$ °C) [42]. When the temperature increases from 22.1 °C to 37.2 °C, intermolecular hydrogen bonds will be weakened, and the PMAA chains will undergo a transition from a highly compact conformation to an expanded coil conformation, resulting in the swelling up of the hybrid nanogels.

While the environmental pH change can induce the volume phase transitions of the hybrid nanogels, it is extremely important to understand whether the morphology and composition of the hybrid nanogels are stable in the different environments for designed functions. Human blood has a normal pH of about 7.4. However, the production of lactic acid under anaerobic conditions

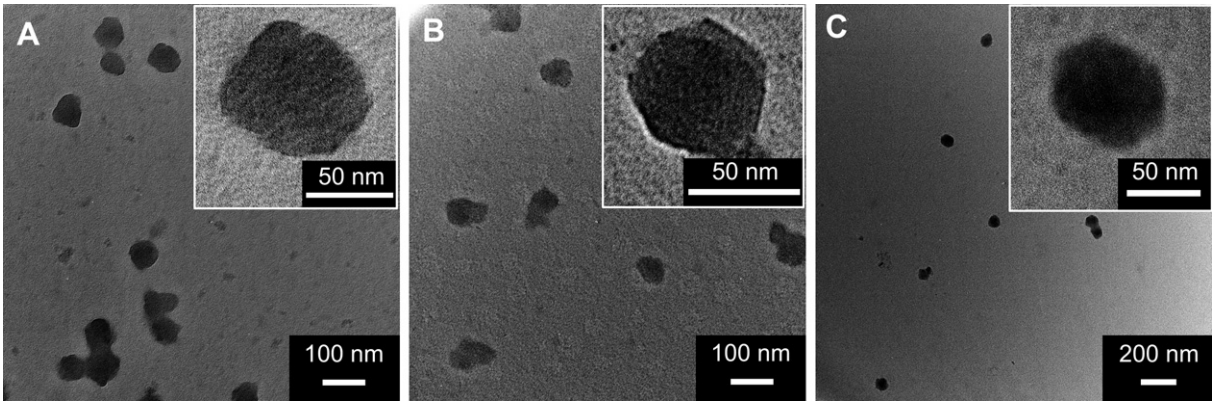


**Fig. 3.** TEM images showing morphology of the as-synthesized chitosan–PMAA–CdSe hybrid nanogels CPM1 (A), CPM2 (B), and CPM3 (C), respectively, in acid medium (pH ~ 5.0).

and the hydrolysis of ATP in an energy-deficient environment contribute to an acidic microenvironment, which has been found in many types of tumors [30]. Thus, the hybrid nanogels as a multifunctional drug carrier would experience the varying environments with a delicate range of acid–alkaline balance (5–7.4) [29–31] if they were used in living systems for *in vivo* diagnosis and therapy. Although the colloidal stability (dispersibility) of the multifunctional bionanoparticles has been widely considered, very limited studies have been carried out to examine the morphology/composition change of the bionanomaterials when subjected to varying environments. Herein, we conducted an experiment, at a proof-of-concept stage, to give some insight into the evolution of the hybrid nanogels during a time period of 32 h, which is longer than the time period (20 h) required for macromolecular drug carriers to accumulate in solid tumors though the blood stream [47]. We found that the hybrid nanogels CPM1 and CPM2 with good entanglement of chitosan chains in the covalently crosslinked PMAA networks were very stable in both dispersibility and morphology/composition when subjected to varying pH environments from 4.8 to 7.38 over the 32 h period. The CdSe QDs were not released from the nanogels due to the strong interaction of CdSe QDs with the –OH groups of chitosan and the ionized $-COO^-$ groups of PMAA chains. In contrast, a significant change in both morphology and composition was observed for CPM3, in which the PMAA chains were not chemically crosslinked. Fig. 6 shows the TEM images (A) and FTIR spectra (B) of CPM3 after exposed to the PBS of pH = 7.38 for 5 h, 10 h, 22 h, and 32 h, respectively, which illustrates how the uncrosslinked PMAA chains gradually released from CPM3 hybrid nanogel particles. The CPM3 nanogels started to swell at pH = 7.38, and then cracked after a certain period (e.g., ≥5 h). This crack further propagated over the extended time period, leading to a demolition of the nanogel and a release of the encapsulated PMAA chains, resulting in seajelly like morphologies of QD-riched structures stabilized by chitosan ribbons. Correspondingly, the intensity of the characteristic FTIR peak of the –COOH groups (1718 $cm^{-1}$) gradually weakened and eventually nearly disappeared at 32 h. The Mw of the polymer chains in the releasing medium was estimated to be about 6000–10,800 Da by using light scattering. Chain expulsion from polyelectrolyte multilayers (PEMs) has been observed for hydrogen-bonded systems as a result of a complete disruption of hydrogen bonds [48]. The pH-triggered diffusion of polyelectrolyte chains in and out of electrostatically assembled PEM film has been reported [49] and fundamentally interpreted [50,51]. Here, we present the first direct observation of the pH-induced expulsion of PMAA chains from the physically associated hybrid nanogels. The mechanism of

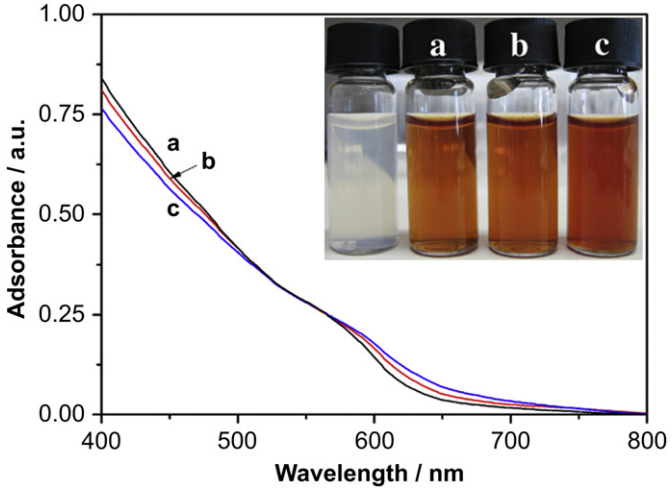


**Fig. 4.** UV–vis absorption spectra of the as-synthesized chitosan–PMAA–CdSe hybrid nanogels CPM1 (a), CPM2 (b), and CPM3 (c), respectively, in acid medium (pH ~ 5.0). The photograph presents the color of the hybrid nanogels. The photograph of chitosan–PMAA nanogel without QDs, showing opalescent color, was also presented for a comparison.

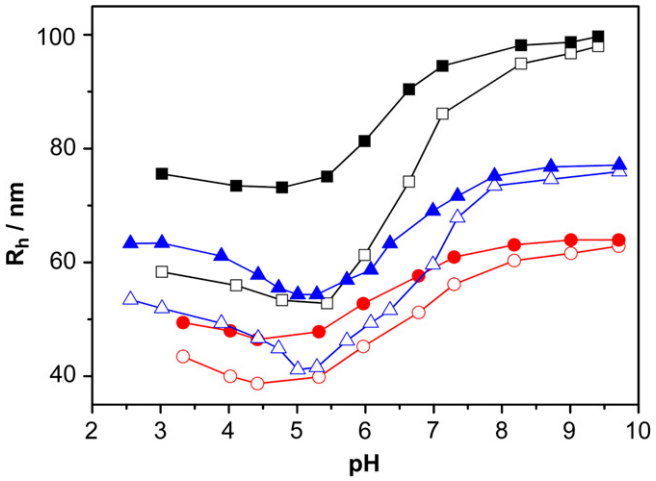


**Fig. 5.** pH dependence of the average $R_h$ value of the chitosan–PMAA–CdSe hybrid nanogels CPM1 (■, □), CPM2 (●, ○), and CPM3 (▲, △), measured at 37.2 °C (solid) and 22.1 °C (open), respectively, and a scattering angle $\theta = 45°$.

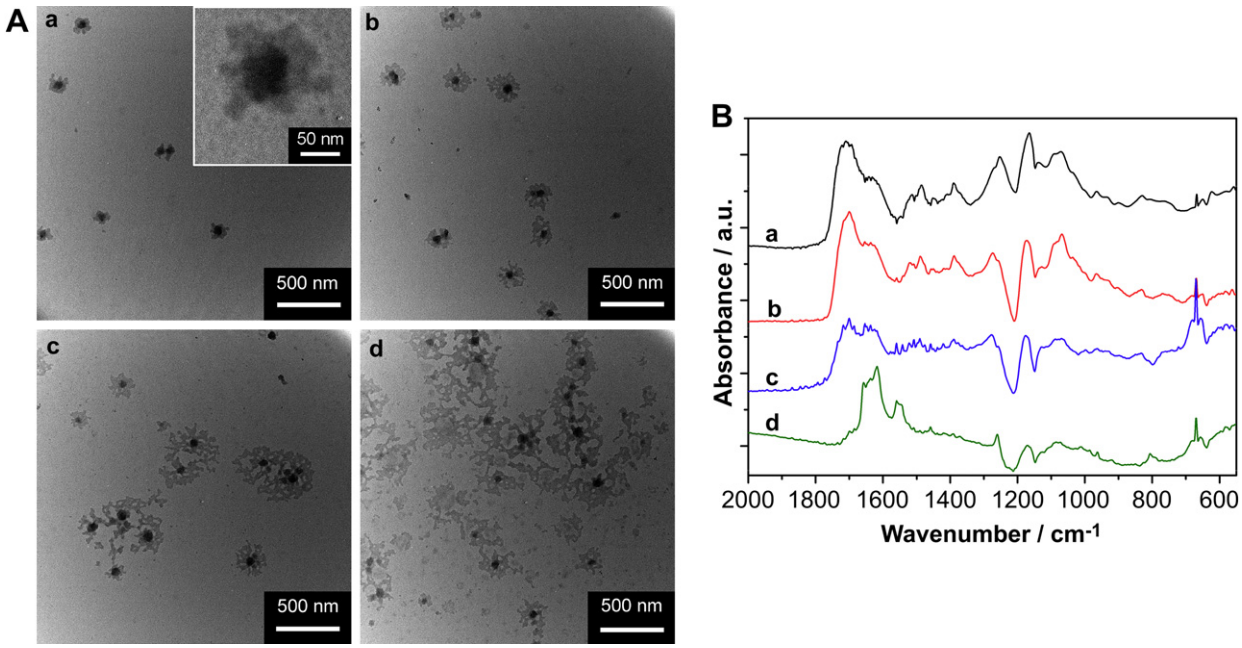


**Fig. 6.** (A) TEM images and (B) FTIR spectra showing the evolvement of the MBAAm-free chitosan–PMAA–CdSe hybrid nanogels CPM3 after dialysis in pH = 7.38 PBS at 37 °C for (a) 5 h, (b) 10 h, (c) 22 h, and (d) 32 h.

chain expulsion of the weak polyelectrolyte nanogels in response to a pH variation may involve pH-induced accumulation of excess charge within the nanogels. This phenomenon could provide fundamental guidance for the construction of feasible and reliable multifunctional bionanomaterials on the basis of chitosan and other biopolymers.

### 3.3. pH-sensitive PL properties of chitosan–PMAA–CdSe hybrid nanogels

Fig. 7 shows the PL spectra of the chitosan–PMAA–CdSe hybrid nanogels dispersed in PBS of different pH values, obtained after equilibrated for 30 min at room temperature. The template

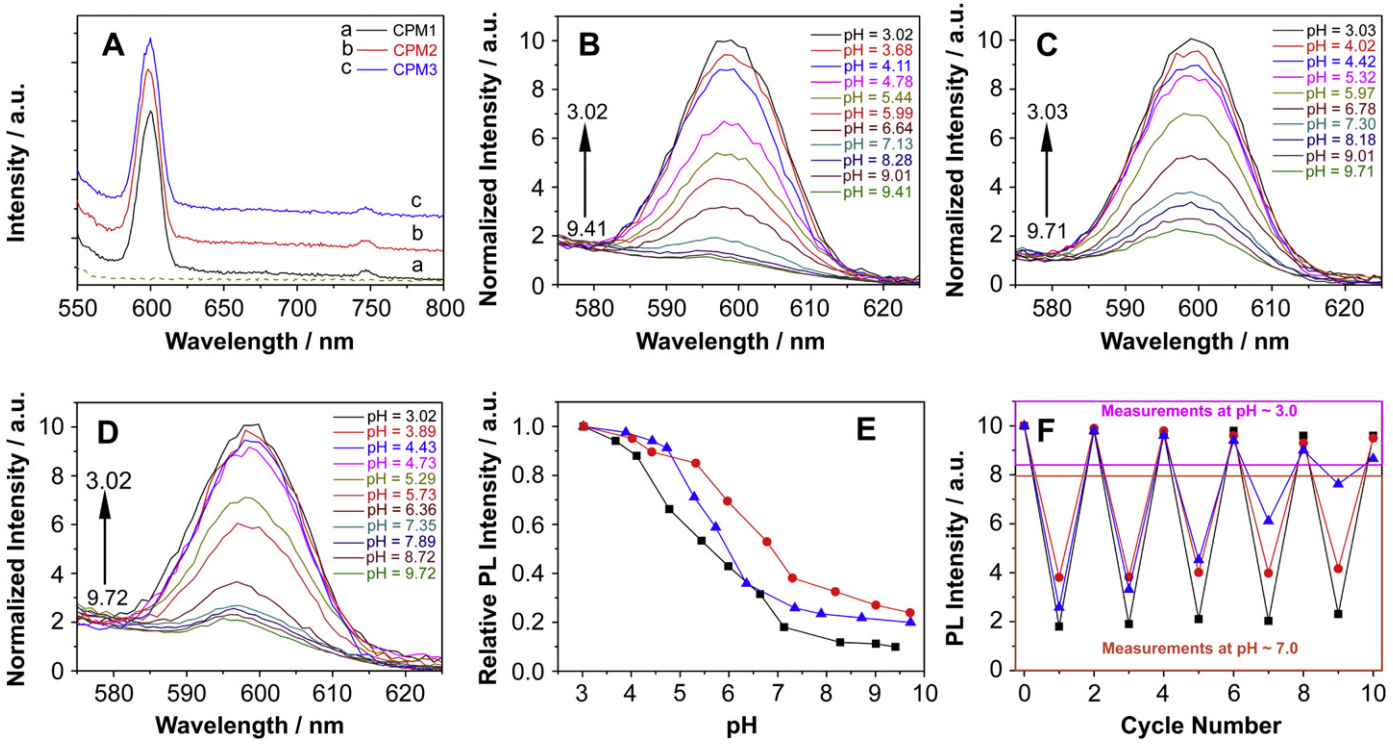


**Fig. 7.** (A) The typical PL spectra of the as-synthesized chitosan–PMAA–CdSe hybrid nanogels obtained with the excitation wavelength at 520 nm. The PL spectrum of the chitosan–PMAA nanogels was also presented for comparison (dot line). (B–D) The pH dependent normalized PL spectra of the CPM1 (B), CPM2 (C), and CPM3 (D) hybrid nanogels, respectively. (E) The relative PL intensity at 599 nm of the CPM1 (■), CPM2 (●), and CPM3 (▲) hybrid nanogels as a function of the pH of surrounding media. (F) PL intensity measured during repeated 5 h' dialysis and pH adjustment cycles of the hybrid nanogels of CPM1 (■), CPM2 (●), and CPM3 (▲), respectively.

chitosan–PMAA nanogels are not fluorescent. After immobilization of CdSe QDs in the interior of the nanogels, a strong red colored emission centered at about 599 nm and a very weak near-IR emission centered at about 743 nm were respectively observed for all the three hybrid nanogels. The emission (599 nm) near absorption edge is related to the excitonic recombination (i.e. charge-carrier recombination) at the band edge, similar to the theoretical exciton energy as modeled on an isolated CdSe nanocrystal of 3.2–3.8 nm within the framework of the pseudopotentical method [52]. The quantum yield of the 599 nm emission was determined to be 19.5%, 22.3%, and 23.1% for CPM1, CPM2 and CPM3, respectively. The quantum yield is appreciably high, in line with those (~9%) normally found in such QDs [53,54], but far below that (~40%) reported by Peng et al. [55], which is possibly associated with the different synthetic methods and the effect of the coating media on the optical electric field at the CdSe QD surface. In agreement with the strong excitonic emission, on the other hand, the emission centre at 743 nm associated with the emissive surface-trap states [52,53] is very weak. The high quantum yield of the QDs should favor their application as optical codes.

The chitosan–PMAA–CdSe hybrid nanogels, combining the properties from both CdSe QDs and responsive polymers, could offer the possibilities for external switching and manipulation. Fig. 7B–D depicts the evolution of the visible excitonic emission (599 nm) of the three hybrid nanogels at various pH values, covering the physiologically important pH range 5–7.4. It is clear that the intensity (quantum efficiency) of the visible excitonic emission could be sufficiently manipulated by varying the pH value of the dispersion. To visualize the relationship between the pH-induced volume phase transitions and the variety in the PL intensity of the chitosan–PMAA–CdSe hybrid nanogels, we plotted the relative PL intensity as a function of pH (Fig. 7E). The comparison of Fig. 5A with Fig. 7E indicates that the PL intensity of the QDs is conspicuously quenched as the nanogels begin to swell at pH $> \sim 5$, and then reaches nearly a constant when the nanogels reach a maximum swelling at pH $> 8$. The pH sensitivity of the PL quenching of QDs can be further tuned through tailoring the swelling degree of the hybrid nanogels. Two factors should be considered to explain how the pH-induced swelling of the nanogels could trigger the PL quenching of the CdSe QDs immobilized in the hybrid nanogels [29]. One is related to the change of the bonding interaction at the surface of CdSe QDs. The increase in pH increases the number of dissociated $-COO^-$ groups and reduces $-NH_3^+$ groups, which cannot only affect the overall swelling/shrinking of the gel network that changes the local dielectric environment surrounding the CdSe QDs, but also involve the exchange in coordinate bonds with the CdSe QDs. This may cause a change of the local optical electric field at the CdSe QD surface, resulting in the PL quenching [29,56]. On the other hand, the increase in the interfacial emission quenching centers can provide the second scenario for the pH-induced PL quenching of CdSe QDs. The increase in pH increases the number of dissociated $-COO^-$ groups of PMAA chains. While the ionized PMAA network chains tend to expand, the crosslinkage of the polymer chains hinders the network expansion, creating elastic tensions localized at the crosslinking points [57]. Because of the bonding between the polymers and CdSe QDs, the CdSe QDs also act as crosslinking points, introducing an elastic tension in the bonds that stretch the polymer/CdSe interface and create interfacial PL quenching states. Wuister's group [58] has reported similar phenomenon, where the frozen solvent induces strain in the capping shell that is further propagated to the surface of the QDs, creating interfacial quenching states.

The pH-responsive PL property of these hybrid nanogels could be potentially used for sensing the acidified endosomes and lysosomes [29–32]. To estimate the reversibility and reliability of the pH-induced PL change, the PL spectra of hybrid nanogels were measured for 5 cycles with a pH adjustment between 3.0 and 7.0 through dialysis against the buffer solution of designed pH for 5 h (Fig. 7F). A slight drop in the PL intensity at pH $\approx$ 3.0 (return to about 85–95% of the original intensity at the fifth cycle) was observed for all the three hybrid nanogels, possibly due to the population change of nonradiative loss paths caused by the dynamic motions of the capping polymer chains [17–22,56]. Nevertheless, both the covalently crosslinked CPM1 and CPM2 showed a well reproductive pH-sensitive PL property over the examined cycles, due to their stability in both dispersibility and morphology/composition. These systems may be ideally applied in the native environment of the more hypoxic/anaerobic vascularized tumor models which have pH difference and an acidic microenvironment [29–32]. However, a dramatic decrease in the pH sensitivity of PL property was observed for CPM3 hybrid nanogels after repeating the dialysis/pH adjustment cycles. The sustained decay in the pH sensitivity of CPM3 hybrid nanogels can be essentially associated with the pH-induced crack of this hybrid nanogel and corresponding release of the PMAA chains as demonstrated in Fig. 6. Clearly, the structural variations of the hybrid nanogels were accompanied by the corresponding optical property changes. An appropriate covalent crosslinkage of the template nanogels should be beneficial to the structure stability and reversible optical property for biosensing application of the hybrid nanogels.

### 3.4. Tumour cell imaging

It is worth to mention that the fluorescence of the hybrid nanogels would not completely quench even at extreme pH environments, thus the hybrid nanogels can be applied for cell-labeling under physiologically important pH conditions. Fig. 8 shows the luminescence images of the mouse melanoma cells B16F10 after stained with the chitosan–PMAA–CdSe hybrid nanogels for 2 h. It is clear that the B16F10 cells can readily phagocytose the small-sized hybrid nanogels. The bright spots are attributed to the CdSe QDs encapsulated inside the chitosan–PMAA nanogels, which can illuminate the entire cell. These bright spots are mainly distributed in the cytoplasm and perinuclear region of the cells. It is thus obvious that these probes do not give dark regions in the cell, and simply areas where the nanogel did not permeate are clear, rendering the chitosan–PMAA–CdSe hybrid nanogels suitable for cell-labeling markers. Although nowadays semiconductor QDs have been widely applied for cellular imaging [1–13], such a chitosan–QD hybrid nanogel system designed for the optical probe would potentially facilitate a simultaneous combination of optical diagnosis, distribution of polymeric drug carriers, and monitoring on the response to drug treatments.

### 3.5. Drug storage and pH-regulated release properties

Having demonstrated the pH-sensing and cellular imaging functions, we further examined the drug storage and delivery abilities of the chitosan–PMAA–CdSe hybrid nanogels under typical administration conditions. TMZ, a new imidazole tetrazinone compound with promising preclinical and clinical activity in nitrosourea-sensitive and nitrosourea-resistant models and manageable toxicity in phase I/II clinical trials [59–62], was selected as a model drug. TMZ undergoes a chemical degradation at physiological pH to form the cytotoxic triazene, an active metabolite of dacarbazine (DTIC), which may represent a more favorable prodrug than DTIC. The degradation product of TMZ (absorption peak at 328 nm) raises a new UV–vis absorption peak

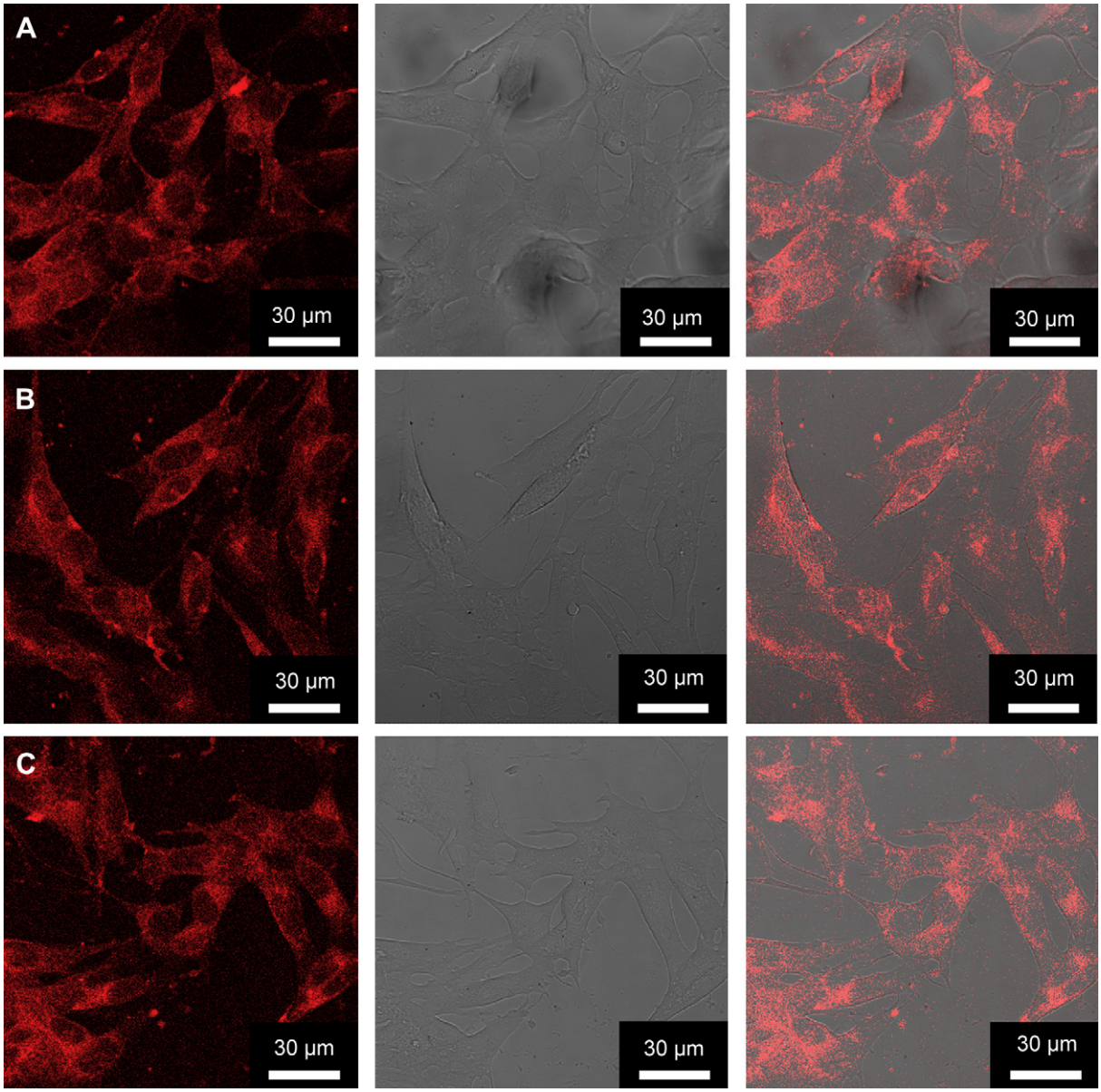


**Fig. 8.** Scanning confocal fluorescence (left), transmission (middle), and overlaid (right) images of mouse melanoma B16F10 cells upon staining with hybrid nanogels CPM1 (A), CPM2 (B), and CPM3 (C), respectively. Excitation wavelength = 496 nm.

at ~266 nm. However, the degradation is negligible at pH $\leq$ 5 [59]. We loaded the well-dissolved TMZ molecules into the hybrid nanogels at acidic pH around 4.3. The addition of TMZ solution into the hybrid nanogels led to an immediate cloudy, which revealed the hydrogen bonding complexation of the amide groups in TMZ molecules with the −OH and protonated −COOH groups in hybrid nanogels. The attractive interactions between the TMZ molecules and the polymer chain networks resulted in a high drug loading capacity and a slight decrease in size of the hybrid nanogels (see Supplementary data Fig. S1). A drug loading capacity of 48.9 wt%, 41.1 wt%, and 38.3 wt%, and the corresponding loading efficiency of 46.4 wt%, 29.4 wt%, and 31.6 wt% were determined for hybrid nanogel CPM1, CPM2 and CPM3, respectively. The confocal images indicate that the drug-loaded hybrid nanogels still show strong fluorescence. The loaded drug molecules also have negligible effect on the pH-sensitive PL property of the embedded QDs.

The drug release from the hybrid nanogels was determined in buffer solutions of different pH values (5.03, 6.17, 6.67, and 7.38) at 37 °C (Fig. 9). A blank release experiment of free TMZ solution with an equivalent amount of drug (46.4 μg/mL) to that trapped in CPM1 was also performed at pH = 7.38. The much slower drug release from the hybrid nanogels than from the free drug solution indicates a sustained release of the TMZ molecules from the hybrid nanogels. First, the change in pH of the releasing medium can trigger the drug releasing rate. The increase in pH induces a gradual dissociation of the −COOH groups to form $-COO^-$ groups, which will not only break the PMAA–TMZ hydrogen bond complexes and enhance the mobility of TMZ molecules, but also increases the swelling degree (mesh size) of the nanogels so that the guest TMZ molecules can diffuse out more easily from the nanogels. Second, a slower release rate was observed on the relatively more crosslinked hybrid nanogels CPM2 which exhibited a smaller swelling ratio as compared with CPM1. Third, TMZ

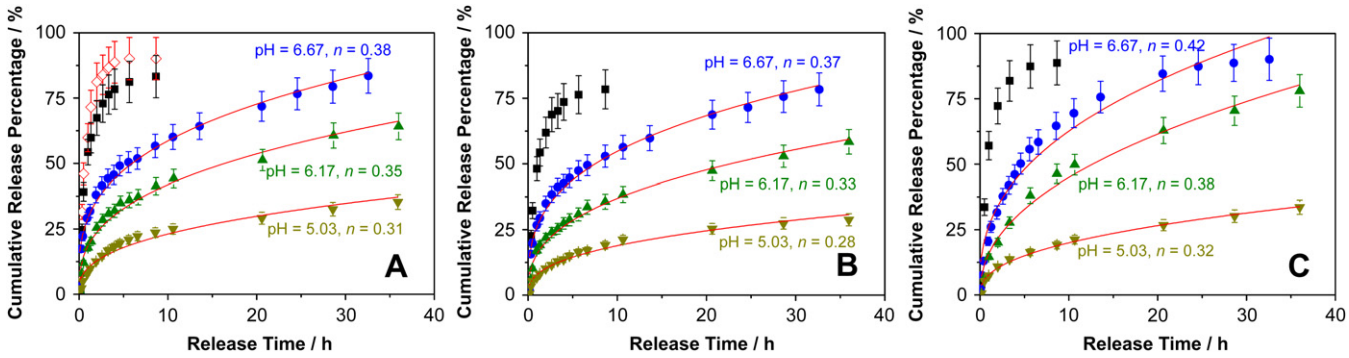


**Fig. 9.** Typical release profile of TMZ from the hybrid nanogels CPM1 (A), CPM2 (B), and CPM3 (C) at 37 °C in PBS solutions of varying pH: (■)-pH 7.38; (●)-pH 6.67; (▲)-pH 6.17; ▼-pH 5.03. In the blank release (◆), 5 mL free TMZ solution was released to 50 mL PBS solution of pH 7.38 at 37 °C. The fitting lines are based on the Empirical Peppas's Model: $M_t/M_\infty = kt^n$.

molecules came out more rapidly from the CPM3 than from the CPM1 and CPM2 hybrid nanogels at pH ≥ 6.17, due to the pH-induced change of both structure and composition of the hybrid nanogel CPM3 (Fig. 6). Moreover, for all the three hybrid nanogels, less than 70% of TMZ loaded into the hybrid nanogels were released in the first 10 h without showing lag phase and zero order release at pH ≤ 6.67.

To further understand the release mechanism, the results were analyzed using the empirical Peppas's model [63] (lines in Fig. 9):

$$M_t/M_\infty = kt^n$$

where $M_t$ and $M_\infty$ are the absolute cumulative amount of drug released to time $t$ and infinite time, respectively, and $k$ is a structural/geometric constant. $n$ is related to the intimate mechanism of release as values of $n < 0.43$ or $n > 0.85$ for a sphere-like device indicate another controlling process in addition to the diffusion process. While the $n = 0.54$ for free TMZ solution indicates an anomalous transportation, the low $n$ values for CPM1 and CPM2 indicated that the release of TMZ molecules obeys to two correlated processes: one is related to the breakage of coordinate hydrogen bonds between the drug and polymer chains; another is a diffusion-controlled step. The same releasing mechanism was found for CPM3 at pH = 6.17 and 5.03, respectively. However, a nearly anomalous transportation of TMZ ($n = 0.42$) was found at pH = 6.67 due to the ionization of PMAA chains and the dissociation of the chitosan–PMAA networks in CPM3. In consistent with the pH-induced PL changes (Fig. 7), the pH-induced drug release

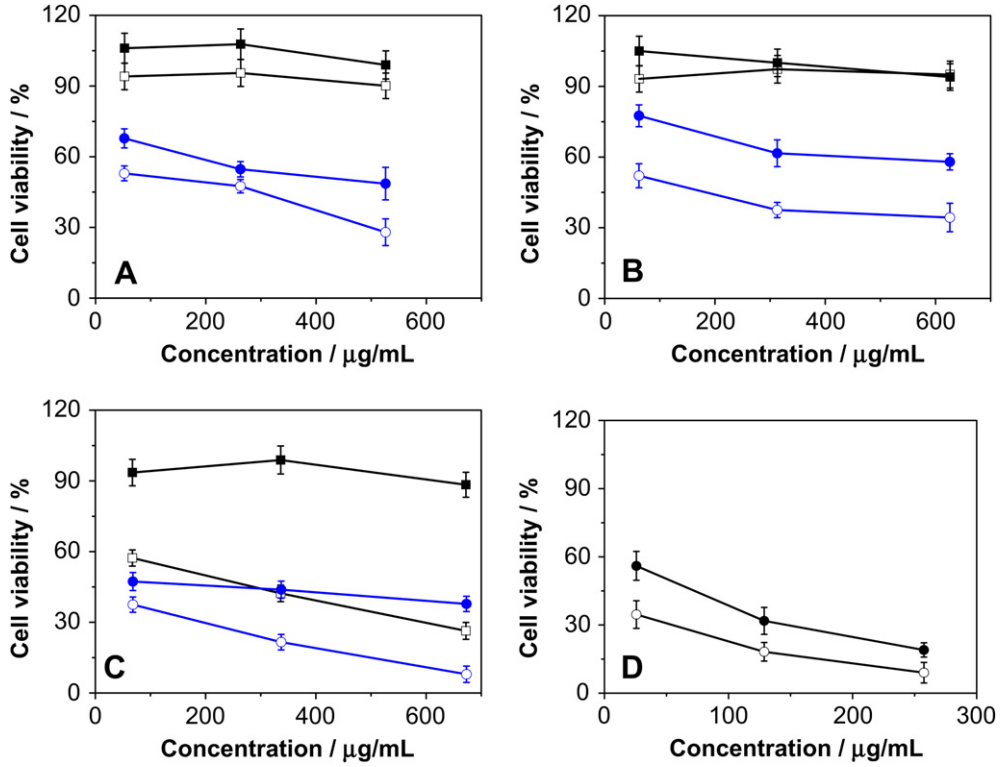


**Fig. 10.** In vitro cytotoxicity of the free chitosan–PMAA–CdSe hybrid nanogels (■) and the TMZ-loaded hybrid nanogels (●) (A: CPM1, B: CPM2, and C: CPM3) against B16F10 cells incubated for 2 h (solid symbols) and 24 h (open symbols), respectively, at different concentrations. (D) The control experiment on the free TMZ was presented for comparison. The concentrations of TMZ solution used for the control study are equal to those of TMZ loaded in the interior of the hybrid nanogels correspondingly.

mechanism change of the hybrid nanogels are essentially regulated by the variations in the structure and properties of the gel networks upon receiving an external stimuli (Figs. 5 and 6).

### 3.6. In vitro cytotoxicity

Although the approach to multifunctional bionanomaterials presents immense opportunities, there are concerns about the safety of these materials following intentional and unintentional human exposures. Fig. 8 shows that no signs of morphological damage to the B16F10 cells were observed upon treatment with the hybrid nanogels for 2 h. This was further confirmed by *in vitro* cytotoxicity results (Fig. 10) that all the free hybrid nanogels were low-cytotoxic to B16F10 cells in the first 2 h in concentrations up to 526.58 μg/mL, 626.52 μg/mL, and 672.30 μg/mL for CPM1, CPM2 and CPM3, respectively. In contrast, the cell viability drastically decreased when the cells were incubated with TMZ-loaded hybrid nanogels for 2 h even at a concentration as low as 52.65 μg/mL, 67.58 μg/mL and 67.23 μg/mL for the TMZ-loaded CPM1, CPM2 and CPM3, respectively (equivalent to about 25.75 μmol/L free TMZ in all systems). Correspondingly, an $IC_{50}$ value of 411.26 μg/mL, 667.54 μg/mL and 68.35 μg/mL was respectively obtained. These results indicate that the released TMZ from the hybrid nanogels can still provide high anticancer activity. Due to the sustained-release property of the TMZ-loaded hybrid nanogels (about 65% of the loaded TMZ was released in 2 h, Fig. 9), the cytotoxicity of TMZ-loaded hybrid nanogels is slightly lower than that of free TMZ at all the studied concentrations.

Upon treatment with free hybrid nanogels for 24 h, the cell viability remains largely unchanged for CPM1 and CPM2, indicating a low-cytotoxicity. However, a drastic decrease in cell viability was observed in the case of CPM3. The reason is that the CPM3 hybrid nanogel has undergone a change in structure and composition to form seajelly like morphologies (Fig. 5C) when exposed to physiological medium for 24 h, leading to the exposure of the relatively bare CdSe QDs to the cells [64]. Our results indicate that appropriate polymer coats on the surface of QDs are feasible strategies to improve the biocompatibility of QDs. While covalently crosslinked hybrid nanogels of CPM1 and CPM2 exhibit a successful combination of optical pH-sensing, regulated drug delivery capabilities, and low-cytotoxicity, the structure/composition change of the physically associated CPM3 hybrid nanogels under physiological conditions have not only immediate consequences for biosensing but also the potential cytotoxicity due to the swelling and release of ionized PMAA chains and exposure of relatively bare QDs to cells. This identification of the potential hazardous material properties could be helpful for the redesign of these bionanomaterials to improve safety while still maintaining or even promoting key nanoscale properties.

## 4. Conclusions

The multifunctional chitosan–PMAA–CdSe hybrid nanogels can be prepared in an aqueous solution via in-situ immobilization of CdSe QDs (3.2–3.8 nm) into the chitosan–PMAA semi-IPN nanogels. The template chitosan–PMAA nanogel can be formed either by non-covalent physical associations, such as secondary forces (hydrogen bonding or hydrophobic association) and physical entanglements, or by covalent crosslinkages. The hybrid nanogels prepared by both methods can sufficiently undergo a pH-induced volume phase transition. Whereas the covalently crosslinked nanogels are very stable in both structure and composition upon pH variation, the hybrid nanogels based on the physical associations exhibit a significant change in the structure and composition in response to a pH increase to physiological condition. This distinction in the stability of hybrid nanogels is important for the designed multiple functions. The results reported here suggest that the covalently crosslinked hybrid nanogels like CPM1 and CPM2 with excellent structural stability and reversible physical property change in response to a pH change can successfully integrate the optical pH-sensing and cellular imaging ability, regulated drug delivery, and low-cytotoxicity into a single nano-object. In contrast, the physically associated hybrid nanogels like CPM3 would not be ideal candidate for biosensing and drug delivery. The hybrid nanogels CPM1 and CPM2 could enter and illumine the B16F10 cells, detect the change in pH, provide a pH-regulated release of anticancer drug TMZ in the typical abnormal pH range of 5–7.4 found in pathological zone, which provides potential for monitoring on the response to drug treatments and improving the therapeutic efficiency. It is important to achieve progress in the development of multifunctional bionanomaterials by incorporation of functional building blocks into a single individual nanoparticle.

## Acknowledgement

We gratefully acknowledge the financial support from the USAID (PGA-P280422) and partial support from PSC-CUNY research award.

## Appendix. Supplementary data

Supplementary data associated with this article can be found, in the online version, at doi:10.1016/j.biomaterials.2010.07.061.

## Appendix

Figures with essential color discrimination. Figs. 1, 2, 4–10 in this article are difficult to interpret in black and white. The full color images can be found in the online version, at doi:10.1016/j.biomaterials.2010.07.061.

## References

[1] Duan HW, Nie SM. Cell-penetrating quantum dots based on multivalent and endosome-disrupting surface coatings. J Am Chem Soc 2007;129:3333–8.
[2] Lim I-IS, Njoki PN, Park HY, Wang X, Wang L, Mott D, et al. Gold and magnetic oxide/gold core/shell nanoparticles as bio-functional nanoprobes. Nanotechnology 2008;19:305102.
[3] Michalet X, Pinaud FF, Bentolila LA, Tsay JM, Doose S, Li JJ, et al. Quantum dots for live cells and in vivo imaging, diagnostics and beyond. Science 2005;307:538–44.
[4] Cui B, Wu C, Chen L, Ramirez A, Mobley WC, Chu S. One at a time: tracking NGF retrograde transport in live neurons. Proc Natl Acad Sci U S A 2007;104:13666–71.
[5] Park K, Lee S, Kang E, Kim K, Choi K, Kwon IC. New generation of multifunctional nanoparticles for cancer imaging and therapy. Adv Funct Mater 2009;19:1553–66.
[6] Bardelang D, Zaman MB, Moudrakovski IL, Pawsey S, Margeson JC, Wang D, et al. Interfacing supramolecular gels and quantum dots with ultrasound: smart photoluminescent dipeptide gels. Adv Mater 2008;20:4517–20.
[7] Zaman MB, Baral T, Zhang JB, Whitfield D, Yu K. Single-domain antibody functionalized CdSe/ZnS quantum dots for cellular imaging of cancer cells. J Phys Chem C 2009;113:496–9.
[8] Kim S, Lim YT, Soltesz EG, De Grand AM, Lee J, Nakayama A, et al. Near-infrared fluorescent type II quantum dots for sentinel lymph node mapping. Nat Biotechnol 2004;22:93–7.
[9] Tan WB, Jiang S, Zhang Y. Quantum-dot based nanoparticles for targeted silencing of HER2/neu gene via RNA interference. Biomaterials 2007;28:1565–71.
[10] Bhang SH, Won N, Lee T, Jin H, Nam J, Park J, et al. Hyaluronic acid–quantum dot conjugates for *in vivo* lymphatic vessel imaging. ACS Nano 2009;3:1389–98.
[11] Lee HA, Imran M, Monteiro-Riviere NA, Colvin VL, Yu WW, Rivlere JE. Biodistribution of quantum dot nanoparticles in perfused skin: evidence of coating dependency and periodicity in arterial extraction. Nano Lett 2007;7:2865–70.

[12] Boussif O, Lezoualch F, Zanta MA, Mergny MD, Scherman D, Demeneix B, et al. A versatile vector for gene and oligonucleotide transfer into cells in culture and in vivo: polyethylenimine. Proc Natl Acad Sci U S A 1995;92:7297–301.
[13] Young SH, Rozengurt E. Qdot nanocrystal conjugates conjugated to bombesin or ANG II label the cognate G protein-coupled receptor in living cells. Am J Physiol, Cell Physiol 2006;290:C728–32.
[14] Zhang J, Xu S, Kumacheva E. Polymer microgels: reactors for semiconductor, metal, and magnetic nanoparticles. J Am Chem Soc 2004;126:7908–14.
[15] Sawant RM, Hurley JP, Salmaso S, Kale A, Tolcheva E, Levchenko TS, et al. "Smart" drug delivery systems: double-targeted pH-responsive pharmaceutical nanocarriers. Bioconjug Chem 2006;17:943–9.
[16] Stuart MAC, Huck WTS, Genzer J, Müller M, Ober C, Stamm M, et al. Emerging applications of stimuli-responsive polymer materials. Nat Mater 2010;9:101–13.
[17] Wu W, Zhou T, Zhou S. Tunable photoluminescence of Ag nanocrystals in multiple-sensitive hybrid microgels. Chem Mater 2009;21:2851–61.
[18] Gong Y, Gao M, Wang D, Mohwald H. Incorporating fluorescent CdTe nanocrystals into a hydrogel via hydrogen bonding: toward fluorescent microspheres with temperature-responsive properties. Chem Mater 2005;17:2648–53.
[19] Guo J, Yang W, Wang C, He J, Chen J. Poly(*N*-isopropylacrylamide)-coated luminescent/magnetic silica microspheres: preparation, characterization, and biomedical applications. Chem Mater 2006;18:5554–62.
[20] Karg M, Pastoriza-Santoz I, Liz-Marzan LM, Hellweg T. A versatile approach for the preparation of thermosensitive PNIPAM core-shell microgels with nanoparticle cores. Chem Phys Chem 2006;7:2298–301.
[21] Jańczewski D, Tomczak N, Han MY, Vancso GJ. Stimulus responsive PNIPAM/QD hybrid microspheres by copolymerization with surface engineered QDs. Macromolecules 2009;42:1801–4.
[22] Wu W, Zhou T, Shen J, Zhou S. Optical detection of glucose by CdS quantum dots immobilized in smart microgels. Chem Commum; 2009:4390–2.
[23] Freiberg S, Zhu XX. Polymer microspheres for controlled drug release. Int J Pharm 2004;282:1–18.
[24] Gautrot JE, Zhu XX. Biodegradable polymers based on bile acids and potential biomedical applications. J Biomater Sci Polym Ed 2006;17:1123–39.
[25] Oh JK, Lee DI, Park JM. Biopolymer-based microgels/nanogels for drug delivery applications. Prog Polym Sci 2009;34:1261–82.
[26] Bhattarai N, Gunn J, Zhang M. Chitosan-based hydrogels for controlled, localized drug delivery. Adv Drug Deliv Rev 2010;62:83–99.
[27] Mao S, Sun W, Kissel T. Chitosan-based formulations for delivery of DNA and siRNA. Adv Drug Deliv Rev 2010;62:12–27.
[28] Zhang L, Gu FX, Chan JM, Wang AZ, Langer RS, Farokhzad OC. Nanoparticles in medicine: therapeutic applications and developments. Clin Pharmacol Ther 2008;83:761–9.
[29] Wu W, Aiello M, Zhou T, Berliner A, Banerjee P, Zhou S. In-situ immobilization of quantum dots in polysaccharide-based nanogels for integration of optical pH-sensing, tumor cell imaging, and drug delivery. Biomaterials 2010;31:3023–31.
[30] Tannock IF, Rotin D. Acid pH in tumors and its potential for therapeutic exploitation. Cancer Res 1989;49:4373–84.
[31] Stubbs M, McSheehy PMJ, Griffiths JR, Bashford CL. Causes and consequences of tumour acidity and implications for treatment. Mol Med Today 2000;6:15–9.
[32] Coakley RD, Grubb BR, Paradiso AM, Gatzy JT, Johnson LG, Kreda SM, et al. Abnormal surface liquid pH regulation by cultured cystic fibrosis bronchial epithelium. Proc Natl Acad Sci U S A 2003;100:16083–8.
[33] Molinaro G, Leroux JC, Damas J, Adam A. Biocompatibility of thermosensitive chitosan-based hydrogels: an in vivo experimental approach to injectable biomaterials. Biomaterials 2002;23:2717–22.
[34] Zaharoff DA, Rogers CJ, Hance KW, Schlom J, Greiner JW. Chitosan solution enhances both humoral and cell-mediated immune responses to subcutaneous vaccination. Vaccine 2007;25:2085–94.
[35] Zaharoff DA, Hoffman BS, Hooper HB, Benjamin CJ, KKm Khueana, Hance KW, et al. Intravesical immunotherapy of superficial bladder cancer with chitosan/interleukin-12. Cancer Res 2009;69:6192–9.
[36] Rogach AL, Kornowski A, Gao M, Eychmüller A, Weller H. Synthesis and characterization of a size series of extremely small thiol-stabilized CdSe nanocrystals. J Phys Chem B 1999;103:3065–9.
[37] Sondi I, Siiman O, Matijević E. Synthesis of CdSe nanoparticles in the presence of aminodextran as stabilizing and capping agent. J Colloid Interface Sci 2004;275:503–7.
[38] Yang YJ, Xiang BJ. Wet synthesis of nearly monodisperse CdSe nanoparticles at room temperatre. J Cryst Growth 2005;284:453–8.
[39] Chu B. Laser light scattering. 2nd ed. New York: Academic Press; 1991.
[40] De Vasconcelos CL, Bezerril PM, Dos Santos DES, Dantas TNC, Pereira MR, Fonseca JLC. Effect of molecular weight and ionic strength on the formation of polyelectrolyte complexes based on poly(methacrylic acid) and chitosan. Biomacromolecules 2006;7:1245–52.
[41] De Vasconcelos CL, Bezerril PM, Dantas TNC, Pereira MR, Fonseca JLC. Adsorption of bovine serum albumin on temperature-polymerized chitosan/poly(methacrylic acid) complexes. Langmuir 2007;23:7687–94.
[42] Zhou S, Chu B. Synthesis and volume phase transition of poly(methacrylic acid-*co*-*N*-isopropylacrylamide) microgel particles in water. J Phys Chem B 1998;102:1364–71.
[43] Alexis F, Pridgen E, Molnar LK, Farokhzad OC. Factors affecting the clearance and biodistribution of polymeric nanoparticles. Mol Pharmacol 2008;5:505–15.
[44] Hobbs SK, Monsky WL, Yuan F, Roberts WG, Griffith L, Torchilin VP, et al. Regulation of transport pathways in tumor vessels: role of tumor type and microenvironment. Proc Natl Acad Sci U S A 1998;95:4607–12.
[45] Lukyanov A, Gao Z, Mazzola L, Torchilin VP. Polyethylene glycol–diacyllipid micelles demonstrate increased accumulation in subcutaneous tumors in mice. Pharm Res 2002;19:1424–9.
[46] Yu WW, Qu L, Guo W, Peng XG. Experimental determination of the extinction coefficient of CdTe, CdSe, and CdS nanocrystals. Chem Mater 2003;15:2854–60.
[47] Matsumura Y, Maeda H. A new concept for macromolecular therapeutics in cancer chemotherapy: mechanism of tumoritropic accumulation of proteins and the antitumor agent smancs. Cancer Res 1986;46:6387–92.
[48] Hiller J, Mendelsohn J, Rubner MF. Reversibly erasable nanoporous antireflection coatings from polyelectrolyte multilayers. Nat Mater 2002;1:59–63.
[49] Picart C, Mutterer J, Richert L, Luo Y, Prestwich GD, Schaaf P, et al. Molecular basis for the explanation of the exponential growth of polyelectrolyte multilayers. Proc Natl Acad Sci U S A 2002;99:12531–5.
[50] Sui ZJ, Schlenoff JB. Phase separations in pH-responsive polyelectrolyte multilayers: charge extrusion versus charge expulsion. Langmuir 2004;20:6026–31.
[51] Kharlampieva E, Ankner JF, Rubinstein M, Sukhishvili SA. pH-Induced release of polyanions from multilayer films. Phys Rev Lett 2008;100:128303.
[52] Rabani E, Hetenyi B, Berne BJ, Brus LE. Electronic properties of CdSe nanocrystals in the absence and presence of a dielectric medium. J Chem Phys 1999;110:5355–69.
[53] Rogach AL, Nagesha D, Ostrander JW, Giersig M, Kotov NA. "Raisin bun"-type composite spheres of silica and semiconductor nanocrystals. Chem Mater 2000;12:2676–85.
[54] Murry CB, Norris DJ, Bawendi MG. Synthesis and characterization of nearly monodisperse CdE (E = sulfur, selenium, tellurium) semiconductor nanocrystallites. J Am Chem Soc 1993;115:8706–15.
[55] Qu LH, Peng XG. Control of photoluminescence properties of CdSe nanocrystals in growth. J Am Chem Soc 2002;124:2049–55.
[56] Myung N, Bae Y, Bard AJ. Enhancement of the photoluminescence of CdSe nanocrystals dispersed in $CHCl_3$ by oxygen passivation of surface states. Nano Lett 2003;3:747–9.
[57] Flory PJ. Principles of polymer chemistry. New York: Cornell University Press; 1953.
[58] Wuister SR, Donegá CM, Meijerink A. Luminescence temperature antiquenching of water-soluble CdTe quantum dots: role of the solvent. J Am Chem Soc 2004;126:10397–402.
[59] Shen F, Decosterd LA, Gander M, Leyvraz S, Biollaz J, Lejeune F. Determination of temozolmide in human plasma and urine by high-performance liquid chromatography after solid-phase extraction. J Chromatogr B 1995;667:291–300.
[60] Saleem A, Brown GD, Brady F, Aboagye EO, Osman S, Luthra SK, et al. Metabolic activation of temozolomide measured *in vivo* using positron emission tomography. Cancer Res 2003;63:2409–15.
[61] Pyrko P, Schönthal AH, Hofman FM, Chen TC, Lee AS. The unfolded protein response regulator GRP78/BiP as a novel target for increasing chemosensitivity in malignant gliomas. Cancer Res 2007;67:9809–16.
[62] Kislin KL, McDonough WS, Eschbacher JM, Armstrong BA, Berens ME. NHERF-1: modulator of glioblastoma cell migration and invasion. Neoplasia 2009;11:377–87.
[63] Peppas NA, Korsmeyer RW. In: Peppas NA, editor. Hydrogels in medicine and pharmacy. Boca Raton, FL: CRC Press; 1987. p. 109.
[64] Lewinski N, Colvin V, Drezek R. Cytotoxicity of nanoparticles. Small 2008;4:26–49.